

RESEARCH PAPER

## Tantalum/ Nitrogen and n-type WO<sub>3</sub> Semiconductor/FTO Structures as a Cathode for the Future of Nanodevices

Siamak Hoseinzadeh <sup>1\*</sup> and Amir Hoshang Ramezani<sup>2</sup>

<sup>1</sup>Young Researchers and Elite Club, West Tehran Branch, Islamic Azad University, Tehran, Iran

<sup>2</sup> Department of Physics, West Tehran Branch, Islamic Azad University, Tehran, Iran

### ARTICLE INFO

#### Article History:

Received 12 October 2018

Accepted 07 December 2018

Published 01 April 2019

#### Keywords:

Cathode

Ion Implantation

Nano Composite

Nano Electronic Devices

Tantalum

### ABSTRACT

In the last decades an extensive number of research papers published on nano chip electrode and cathode electrochromic materials. Tantalum (Ta) with so high melting point can be a immeasurable candidate for the future of nanochip devices. However, its surface has not enough trap centers and occupation states, so nitrogen ions exposed on Ta surface may solve this problem. For this purpose, in the present work, samples of tantalum (99.99%) with 0.58 mm thickness were embedded by nitrogen ions. The ions' implantation manner was operated at 30 keV and also at various doses which were in the range between 10<sup>17</sup>- 10<sup>18</sup> ions/cm<sup>2</sup>. The electrical, nanostructures characteristics, sample surface topography property were investigated on Tantalum nitrides (Ta/N) structures by looking at current-voltage (I-V) curves. In addition to Ta/N, WO<sub>3</sub> powders as a famous Electrochromic (EC) metal oxide, a silver metal deposited on fluorine doped tin oxide (FTO)-coated glass and multilayer structure with using the physical vapor deposition (PVD) apparatus are determined. Some techniques such as UV- visible, Atomic Force Microscopy (AFM) and X-Ray Diffraction (XRD) have been appropriated. The obtained results show the formation of hexagonal tantalum nitride (TaN<sub>0.43</sub>), and more trap centers of the sample surface (in comparison to current cathode material of EC device (ECD)). The electrical resistivity of the tantalum following nitrogen implantation is also perceived to increase with ion doses. Consequently, Ta/N with more trap centers (rough surface) can be suggested as a good element of the future of EC and nanodevices.

### How to cite this article

Hoseinzadeh S, Ramezani AH. Tantalum/ Nitrogen and n-type WO<sub>3</sub> Semiconductor/FTO Structures as a Cathode for the Future of Nanodevices. J Nanostruct, 2019; 9(2): 276-286. DOI: 10.22052/JNS.2019.02.010

### INTRODUCTION

Unspecified nanoelectronic devices such as OFET (Organic field effect transistors), CMOS (Complementary metal oxide semiconductor) transistors, and OLED (organic light emission diode) devices need an electrode amidst the high-grade connection point at in especially carrier's flux tube or channel [1-3]. The other devices, here, the cathode deposited on fluorine-doped tin oxide (FTO) coated glass substrate by PVD (Physical vapor deposition) method, needs more trap centers as well as a cathode for electrochromic (EC) and

nanodevices [4-8].

It is completely apprehended that the nitrogen ion implantation can improve the surface properties of metals by converting their structures and compositions in the surface coatings. Because of this understanding, the nitrogen ion implantation has been investigated for many years, and several nitrogen-metal systems have been studied in classification to clarify the composition ion mechanisms of multiple metal nitrides and their influences on surface properties. The impressions of nitrogen ion implantation (NII)

\* Corresponding Author Email: [hoseinzadeh.siamak@gmail.com](mailto:hoseinzadeh.siamak@gmail.com)



This work is licensed under the Creative Commons Attribution 4.0 International License.

To view a copy of this license, visit <http://creativecommons.org/licenses/by/4.0/>.

on nanostructural, electro-optical properties of various materials have been investigated [9-11]. The degree of surface modification by NII depends on the ion energy, current density, irradiation time and the substrate temperature. Metal nitride coatings have different physical characteristics like melting points and exclusive electrical stability. In this regard, ion implantation is one of the prospective ways for changing chemical and physical properties in the near-surface part of metals by the formation of nitride phases [12-14].

Tantalum nitride (Ta/N) has many attractive characteristics, for instance, high melting point, hardness, chemical stability and thermal conductivity and low electrical resistivity, which make it possible to use as diffusion barriers for suitable cabling classifications in silicon-based integrated circuits (IC) [13-16].

Moreover, TaN can also be manipulated in a spacious variety of applications such as corrosion-resistant materials and high-speed thermal printing head as well as thin film resistors. While Tantalum nitride deposition procedure can be tuned to achieve a wide range of electrical properties variable the film stoichiometry [17-21], as one of the barriers for copper back-end-of-line processing, high resistivity and narrow process window continue to limit the usability of these films as thin film resistors in Silicon IC manufacturing. Belii et al [18] reported Ta<sub>2</sub>N and TaN formation by ion-implantation at a dose of  $1 \times 10^{17}$  ions/cm<sup>2</sup>, while at higher dose of  $5 \times 10^{17}$  ion/cm<sup>2</sup>, only FCC (Face Cubic Center) TaN was identified. They also found that, the electrical resistivity of the implanted layer increases with increasing ion-dose. Wang et al. [19] studied the structure and the composition of nitrogen implanted tantalum at 1-10 keV with a dose of  $5 \times 10^{17}$  ion/cm<sup>2</sup>. Zhou et al. [20] have reported the ion-dose dependence of the structure of the nitrogen implanted tantalum in the range of  $5 \times 10^{16}$  to  $5 \times 10^{17}$  (80 keV energy). Yadav et al. [22] reported the formation of Ta<sub>2</sub>N and TaN<sub>0.8</sub> at all doses and TaN at higher doses ( $5 \times 10^{17}$  ion/cm<sup>2</sup> to  $1 \times 10^{18}$  ion/cm<sup>2</sup>).

Considering tantalum samples, a moderate bombarding dose ( $1 \times 10^{17}$  -  $1 \times 10^{18}$  ions/cm<sup>2</sup>) of medium-energy heavy-ions would be enough for amorphization without producing substantial topographical changes.

In the present work, the surface topography was analyzed with an Atomic Force Microscope (AFM). AFM images show nitrogen ion bombardment of tantalum surfaces induced topographical changes at normal incidence and standard doses. The structure phases of TaN and WO<sub>3</sub> have analyzed with X-ray diffraction (XRD) technique. The energy gap of WO<sub>3</sub>, determined with UV- visible tool, was also found. The obtained results indicate that Ta/N with more trap centers can be identified as a possible element of the subsequent ECD and nanodevices [23-27].

## MATERIALS AND METHODS

The method of ion bombardment was made on samples of tantalum with sizes of 1cm×1cm and 0.58 mm thicknesses by the ion implantation equipment in the Plasma Physics Research Center (PPRC), and at the Science and Research Branch. The Ion bombardment procedure was implemented by nitrogen ions (99.999%) with the energy of 30 keV and doses of  $(1-10) \times 10^{17}$  ion/cm<sup>2</sup> at ambient temperature, while the angle between the implanted ions and surface of samples was 90°. Prior to ion implantation, the sample surfaces were finished in a manner that resulted in a glossy coating using diamond paste. They were then ultrasonically cleaned in alcohol and acetone. The next phase was to dry them in an oven with a 100 °C temperature.

The extracted ions (without mass selection) were accelerated to the maximum energy of 30 keV. Ion beam energy and current densities were kept fixed for all the samples. The samples were implanted at doses of  $1 \times 10^{17}$  to  $10 \times 10^{17}$  ions/cm<sup>2</sup>. It was expected that the ion beam cross-section uniformly cover all the sample area. The implantation parameters have been listed in Table 1. Before starting the ion implantation, the

Table 1. The process parameter during implantation

Sample	Ion current ( $\mu$ A/cm <sup>2</sup> )	Dose (ions/cm <sup>2</sup> )	Time (s)	Vacuum ( $\times 10^{-6}$ )Torr	Temperature (°C)
0	-	Un-implanted			
1	40	$1 \times 10^{17}$	360	2.7	100
2	40	$3 \times 10^{17}$	470	2.7	100
3	40	$5 \times 10^{17}$	700	2.7	100
4	40	$10 \times 10^{17}$	1600	2.7	100

sample was at room temperature. However, this temperature altered during the implantation due to the heat transfer which came from ion bombardment to the samples.

Structural characters and the composition of the samples of tantalum were investigated with various methods. The nano- microstructure of the samples before and after ion implantation and WO<sub>3</sub> crystallite phases were characterized by X-ray diffraction (XRD) analysis. For this purpose, we used the STOE model STADI MP system using Cu k<sub>α</sub> radiation (wavelength = 1.5405 Å) with a tungsten filament at 40 kV, 40 mA and step size of 0.04 and shown in Fig. 1 and Fig. 2.

The implantation-induced modification of

surface roughness and surface topography of WO<sub>3</sub> were studied employing atomic force microscopy (AFM). The facility was an AFM (SPM Auto Probe CP, Park Scientific Instruments, USA) in contact mode with a low-stress Tantalum nitride tip of less than 20 nm radiuses and a tip opening of 18. AFM analysis in contact mode. Resistivity values of tantalum sample were measured at room temperature using four-point probe technique.

Parallel to Ta/ N experiments, for constructing FTO/WO<sub>3</sub>/Ag, Ta/WO<sub>3</sub>/Ag electrochromic (EC) arrangement is deposited toward fluorine-doped tin oxide (FTO) coated glass substrate by physical vapor deposition (PVD) method. Current (Å), deposition time (second) and deposition rate (Å/

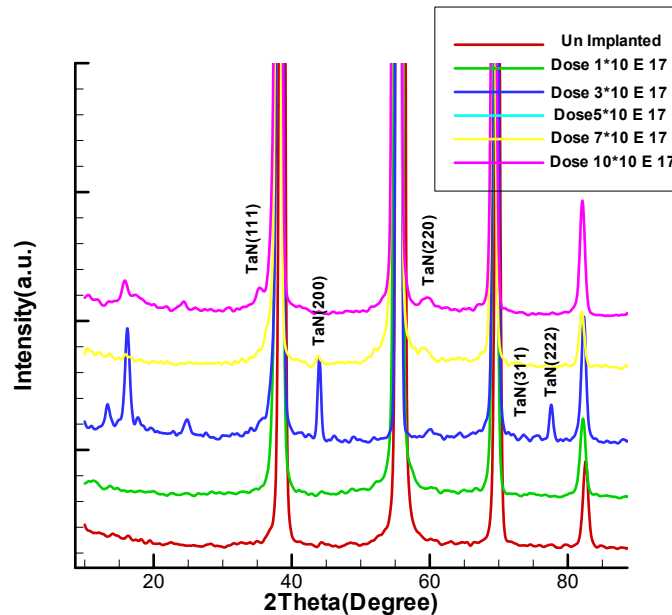


Fig. 1. XRD patterns of samples before and after ion implantation (See also Table 1).

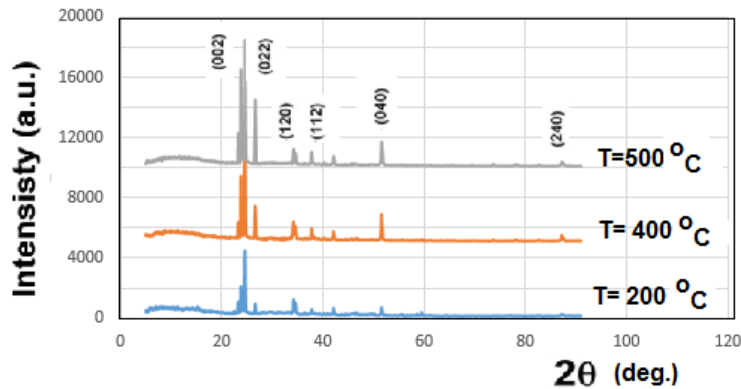


Fig. 2. XRD patterns of WO<sub>3</sub> samples at T= (200, 400 and 500 °C) annealing temperatures

Sec) of PVD is shown in Fig. 3. After passing 40 min of deposition time, the highest deposition rate (0.53 Å/Sec) and 60 min of deposition time, the maximum amount of electrical current (170 A) could be determined.

In this method, first the WO<sub>3</sub> nanoparticles powder with an average rate of 0.4 Ås<sup>-1</sup> are deposited in vacuum on FTO substrate for 80 minutes, and then the Ag nanoparticles powder is deposited on prior layer for 1 minute. In the beginning, WO<sub>3</sub> electrochromic layer with an

average of 0.4 Ås<sup>-1</sup> is deposited on prior layers for 5 minutes. Finally, the layer of Ag nanoparticles is deposited for 1 minute with the rate of 0.1 Ås<sup>-1</sup>. The fabricated electrochromic devices (ECDs) post annealed to investigate the effects of temperature on energy gap of WO<sub>3</sub>. For this purpose, the temperatures of 100, 200 and 500 °C are selected, and ECDs annealed for two minutes in vacuum. The maximum of current was about 3.5 mA in oxidation state for this sample. Furthermore, the change of transmittance for this sample was

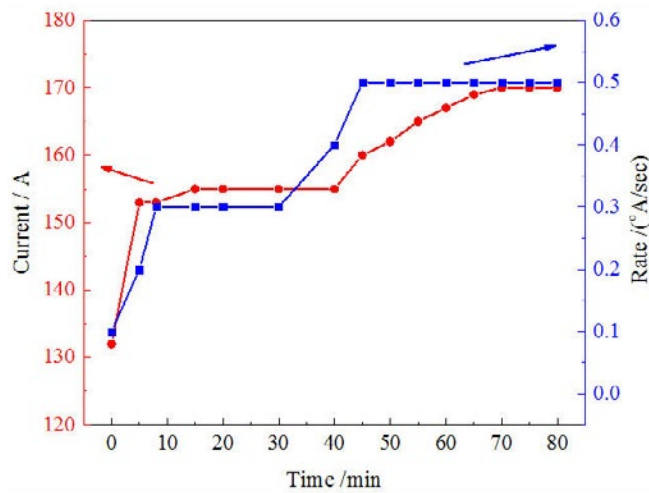


Fig. 3. The curves of current and deposition rate versus time in the deposition process.

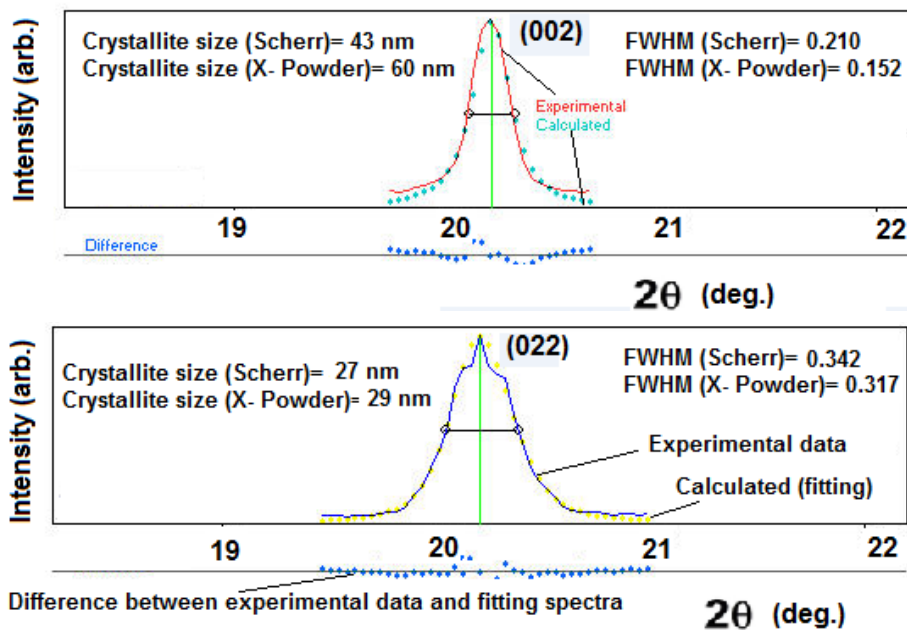


Fig. 4. The size of (up) (002) WO<sub>3</sub> crystallite phase is 43 nm (Scherer) and 60 nm (X- Powder) and (down) (022) WO<sub>3</sub> crystallite phase is 27 nm (Scherer) and 29 nm (X- Powder). FWHM is  $\beta$  in Scherer equation.

upgraded to 40.30% at continuous switching steps. This arrangement (WO<sub>3</sub>/Ag/WO<sub>3</sub>/Ag) can be used in ECDs with its excellent properties.

## RESULTS AND DISCUSSION

### Phases, crystalline structure

Fig. 1 illustrates XRD results of both unimplanted and implanted samples of tantalum as a function of implantation dose. The spectra are limited to the specific region from 24 to 82° for 2θ with four peaks concerning Ta (110), Ta (200), Ta (211) and Ta (200) at different angles of 2θ=38.66, 55.76, 69.82 and 82.50. Nevertheless, ions of high energy, those with doses of 3×10<sup>17</sup> ions/cm<sup>2</sup> and 3×10<sup>17</sup> ions/cm<sup>2</sup> show the TaN<sub>0.43</sub> diffraction peak location in the second and third samples. Aforementioned can be explained by the fact that nitrogen ions take interstitial positions in Tantalum to form Tantalum nitride. According to SRIM simulation, in low ion energy, electron stopping is dominant; nitrogen ions are not able to remove host atoms. In fact, the ions of nitrogen interact with electrons of the host atom in order to break the bonds between Tantalums.

It can be seen that all peaks have changed positions, while a few of them have broadened.

Since constant parameters like temperature, ion density and energy have been applied in all experiments; the peaks' presence depends on the production of conjunctions between Nitrogen and Tantalum due to the increase in the ion dose. The XRD patterns of samples before and after ion implantation have been listed in Table 2. Besides, two dominated peaks of WO<sub>3</sub> powder determined by using x- Powder software are also shown in Fig. 4.

Fig. 1 indicates that peak intensity and substrate broadness for implanted samples have been modified. This increase or decrease in peak intensity can be explained according to the implantation of nitrogen ions on tantalum substrate and the formation of a TaN new phase. It seems that during the process of the formation of phase structures in tantalum, nitrogen atoms get the interstitial positions. This does not result in the creation of sharp boundaries between the nitride and metallic phase structures.

Moreover, as it can be seen in Fig. 1, the diffraction peaks of the substrate are shifted at lower angles (2θ=37.53, 54.44, 68.14 and 80.59) that belong to the diffraction line of the TaN phase (refer to standard card No: #71- 0265).

Table 2. Summary of XRD information and crystallite size of samples

Sample	Position (2θ)	Height (cps)	FWHM (2θ)	h k l index	d-spacing
Un implanted	38.66	1057	0.4723	bccTa	2.329
	55.76	9823	0.4723	bccTa	1.648
	69.82	515	0.4723	bccTa	1.347
	82.50	42	0.6720	bccTa	1.168
1	38.30	1148	0.4330	bccTa	2.349
	55.46	6591	0.4330	bccTa	1.656
	69.49	362	0.4330	bccTa	1.352
	82.29	42	0.4800	bccTa	1.170
2	16	47	0.9646	002 Ta <sub>5</sub> N <sub>6</sub>	6.631
	24.77	6	0.4723	101 Ta <sub>4</sub> N <sub>5</sub>	5.504
	38.39	1324	0.9446	210 TaN <sub>0.43</sub>	3.593
	44.2	57	0.4723	201 TaN <sub>0.43</sub>	2.344
	55.52	1525	0.2755	300 TaN <sub>0.43</sub>	2.056
	69.61	835	0.3936	211 bcc Ta	1.655
	77.59	21	0.3936	311 TaN <sub>0.43</sub>	1.350
	82.34	64	0.4800	202 bcc Ta	1.230
3	24.66	10	0.4723	022 Ta <sub>3</sub> N <sub>5</sub>	3.602
	38.30	1142	0.4723	112 Ta <sub>5</sub> N <sub>6</sub>	2.349
	43.87	34	0.3149	202 Ta <sub>3</sub> N <sub>5</sub>	2.063
	55.43	5002	0.3936	200 bcc. Ta	1.657
	68.47	538	0.3936	211 Ta <sub>3</sub> N <sub>5</sub>	1.352
	82.33	63	0.4800	220 bccTa	1.170
4	38.19	1265	0.4723	110 bcc Ta	2.356
	55.24	4537	0.3936	200 bcc Ta	1.662
	69.33	383	0.4330	211 bcc Ta	1.355
	82.88	59	0.6720	101 bcc Ta <sub>4</sub> N <sub>5</sub>	1.172

The broadening and shift of the peaks are both connected to the phase concerning TaN<sub>0.43</sub> (110) expanded austenite, which was per second produced by the super saturation of nitrogen, as well as the stress which was caused by nitrogen's remaining in the solid solution of the lattice. Furthermore, another three additional peaks are observed by increasing nitrogen doses from 1×10<sup>17</sup> ions/cm<sup>2</sup> to 3×10<sup>17</sup> ions/cm<sup>2</sup> which relate to the nitride phase. This fact confirmed the start of the nitride forming phase where the structures are amorphous in low dose. Also, increasing the dose further to 5×10<sup>17</sup> ions/cm<sup>2</sup>, the intensity of TaN<sub>0.43</sub> (201) and TaN<sub>0.43</sub> (300) diffraction peaks increases. This is while for doses 7×10<sup>17</sup> and 10×10<sup>17</sup> ions/cm<sup>2</sup>, the diffraction peaks of TaN<sub>0.43</sub> with conversion to

amorphous structures, are reduced. In addition, decreasing and increasing roughness in the dose of 1×10<sup>17</sup> ions/cm<sup>2</sup> might happen by an increase in the values of surface dispersion of tantalum atoms on the sample's surface. Moreover, by increasing the ion's dose, the intensity of TaN<sub>0.43</sub> diffraction peaks changes. This phenomenon can be the result of structural defects of the surface sample caused by ion bombardment. Thus, variation in surface roughness results in a non-uniform corrosion of the samples. Noteworthy to mention is that when low density is considered, there are no changes in tantalum structure. Nevertheless, the angles have reduced, thus the space between the two plans increased, and nitrogen atoms have been placed among tantalum atoms. The rise in peak intensity

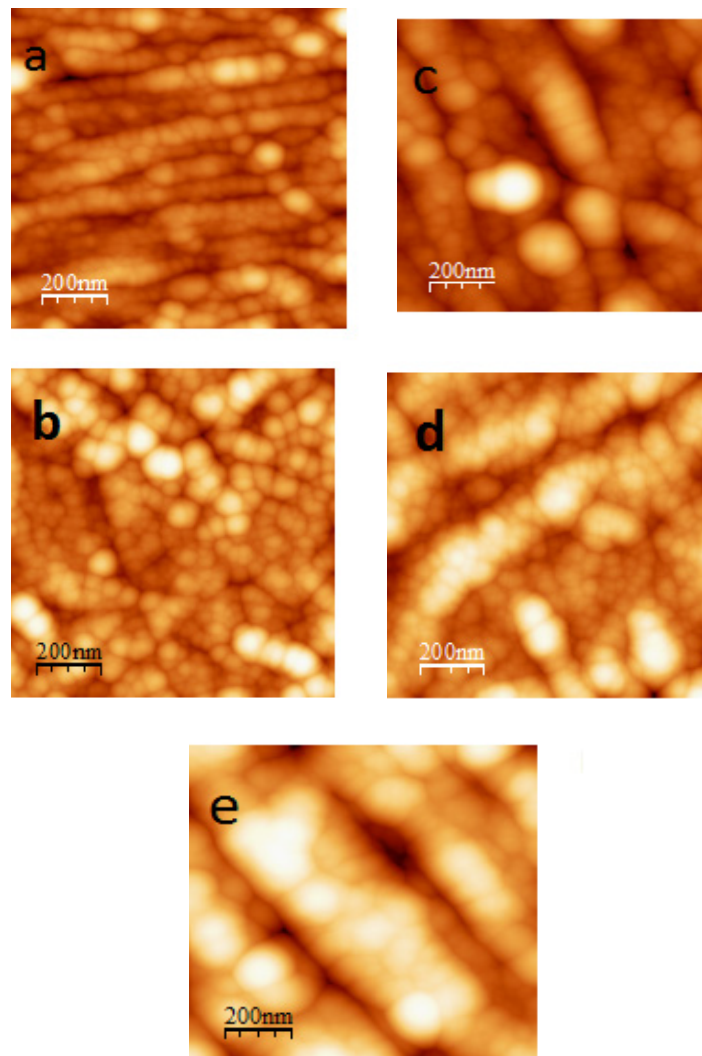


Fig. 5. 2D AFM images of unimplanted and nitrogen ion implanted Ta; a) unimplanted, b) 1× 10<sup>17</sup> ion/cm<sup>2</sup>, c) 3× 10<sup>17</sup> ion/cm<sup>2</sup>, d) 5× 10<sup>17</sup> ion/cm<sup>2</sup>, e) 1× 10<sup>18</sup> ion/cm<sup>2</sup>

is connected to the increase in nitrogen atoms as well as the likelihood of the existence of a bond between nitrogen and tantalum atoms.

*Surface morphology, and roughness*

The Surface roughness of the samples will undergo a substantial change after bombardment. As stated before, AFM is used for the investigation of surface topography as well as the roughness of Ta/N (Fig. 5) and WO<sub>3</sub> (Fig. 6) sample surface. As an example of DM-SPM software for measuring surface roughness is shown in Fig. 7 and the

measurement data are invested in Tables 3 and 4. Fig. 8 also reveals roughness variation curve. Fig. 8 exhibits that by increasing the implantation dose, the topography and the size of grains on the samples change.

The surface roughness, as a statistical property of a surface, is described with DMSPM software image and data (See Fig. 7). There are many various parameters: The surface root-mean-squared roughness in nm<sup>2</sup> (S<sub>a</sub>), Mean in nm (S<sub>m</sub>), two orientation roughness values (S<sub>y</sub>, S<sub>z</sub>) which show y-z (the Peak-Valley Height) plane are also measured and Root Mean Square (S<sub>q</sub>). These are calculated from the data according to the following formulas (1-3) [28, 29]:

$$S_a = \frac{1}{N} \sum_{i=0}^{N-1} |z(x_i)| \tag{1}$$

Table 3: Roughness parameters for WO<sub>3</sub>

Sy	28.3 nm
Sz	22.5 nm
Sa	2.01 nm
Sq	3.29 nm
Sm	10.8 pm

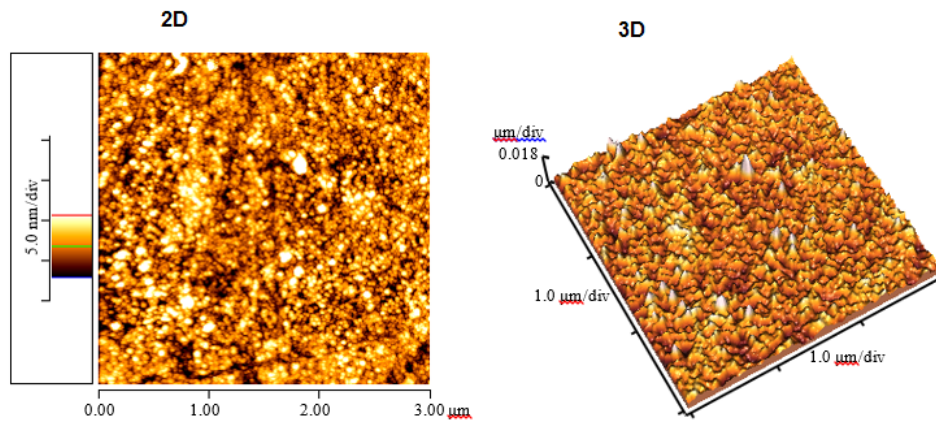


Fig. 6. 2D and 3D AFM images of WO<sub>3</sub> at 500°C annealing temperature

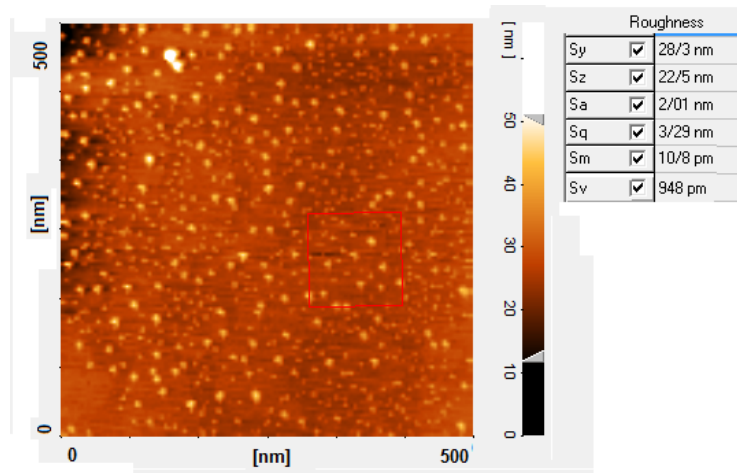


Fig. 7. The surface roughness parameters of WO<sub>3</sub> (at 500°C annealing temperature) are measured with DM-SPM software

$$S_m = \frac{1}{N} \sum_{l=0}^{N-1} z(x_l) \quad (2)$$

$$S_q = \sqrt{\frac{1}{N} \sum_{l=0}^{N-1} (z(x_l))^2} \quad (3)$$

Table (3) summarizes the roughness parameters of WO<sub>3</sub> nanoparticles obtained from DM- SPM software.

By comparing the values of WO<sub>3</sub> sample roughness parameters obtained from DMSPM software (data are given in Table (3)), and Ta/N with exposing to 10×10<sup>17</sup> nitrogen ions per cm<sup>2</sup>, show different surface topography.

Moreover, as can be seen from Table 4, by increasing the ion dose to 3×10<sup>17</sup> and 10×10<sup>17</sup> ions/cm<sup>2</sup>, the surface roughness of the Tantalum is significantly raised. It seems that by entering nitrogen ions into the surface, the etching process has occurred.

On the other hand, surface diffusion processes, due to ion bombardment, increase the surface roughness at higher doses (10×10<sup>17</sup> ions/cm<sup>2</sup>).

Also, at the highest implantation dose (10×10<sup>17</sup> ions/cm<sup>2</sup>), some grooving development effect dominates the diffusion and roughness enhances. Fig. 5 shows the root mean square (RMS) roughness and average roughness un-implanted and some of the implanted samples. It is clear from Fig. 8, that with increasing the dose from 1×10<sup>17</sup> ions/cm<sup>2</sup> - 10×10<sup>17</sup> ions/cm<sup>2</sup> with variations in surface roughness, the grains size formed on the surface is also changed. The result shows that the surface roughness increases with nitrogen ion doses. The AFM images show that there is an increase in the RMS roughness of the sample's surface with an increasing dose. The surface diffusion mechanism, due to a greater number of ions in the implantation process, is responsible for this change.

*Electrical resistivity*

The square resistance (R) of all films was also measured using the four-point-probe method. Electrical resistivity (ρ) was obtained from the sheet resistance and film thickness from the following relation: ρ = R<sub>s</sub> t Where ρ is resistivity

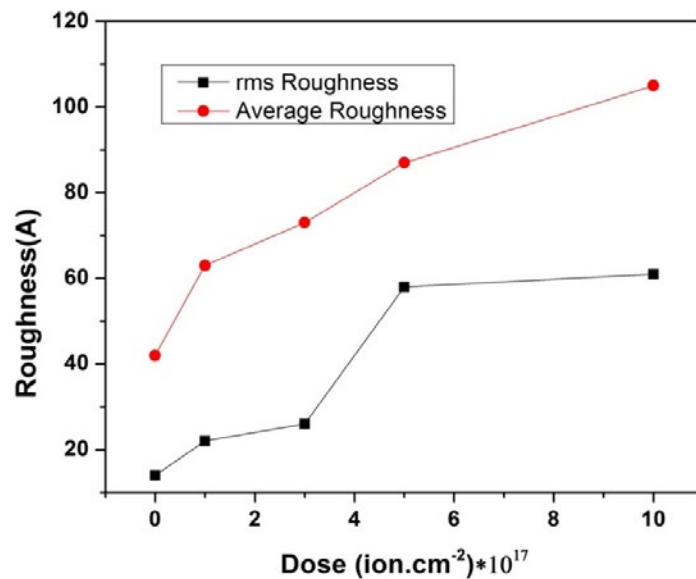


Fig. 8. Average and rms surface roughness of unimplanted and nitrogen ion implanted Ta.

Table 4. Structural and electrical data of Ta/N sample surface.

Sample	(S <sub>q</sub> ) [nm]	S <sub>a</sub> [nm]	S <sub>m</sub> (nm)	ρ (mΩ.cm)
Un implanted	1.42	4.19	8.55	182.7
1	2.23	6.13	36.1	197.2
2	3.54	7.25	10.6	220.4
3	5.93	8.22	5.5	243.6
4	6.34	10.52	9.2	272.6



(Ω.cm), and t is thickness from SEM (cm) [30- 40].

Fig. 9 shows the results of electrical resistivity measurements at room temperature that there is an improvement in the electrical resistivity of the sample's surface with a growing dose. According to our laboratory results, a robust relationship between the resistivity and the RMS roughness can be perceived. According to Fig. 8 with increasing the surface roughness the resistivity values improvements. The nitrogen ion implantation

causes the structural and compositional variations in the modified surface layer, and that is why the electrical resistivity can be developed. Table 4, shows the extent of improvement in resistivity with the increase of ion doses.

Indeed, the resistivity values for the tantalum acquired using ion implantation technique have been in a range of 182-272 mΩ.cm. It can be seen that the electrical resistivity for the tantalum which doses  $10 \times 10^{17}$  ion/cm<sup>2</sup>, had a high value of 272

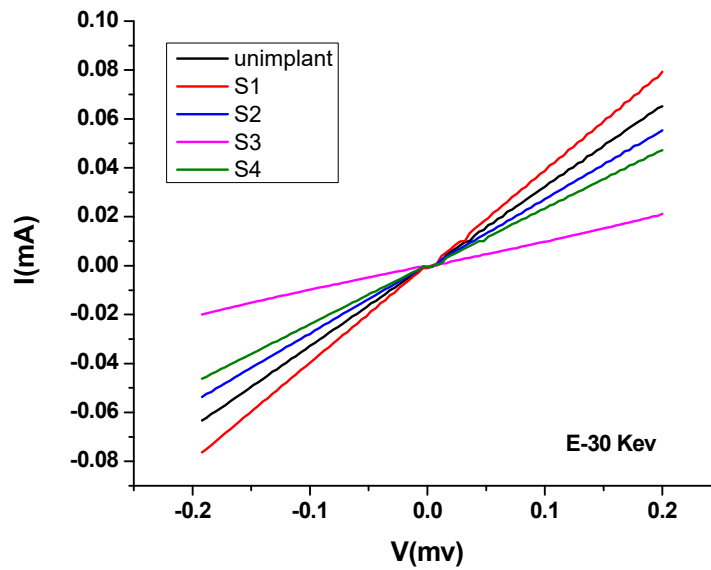


Fig. 9. Variation of voltage as a function of current for unplanted and Nitrogen ion implanted Ta.

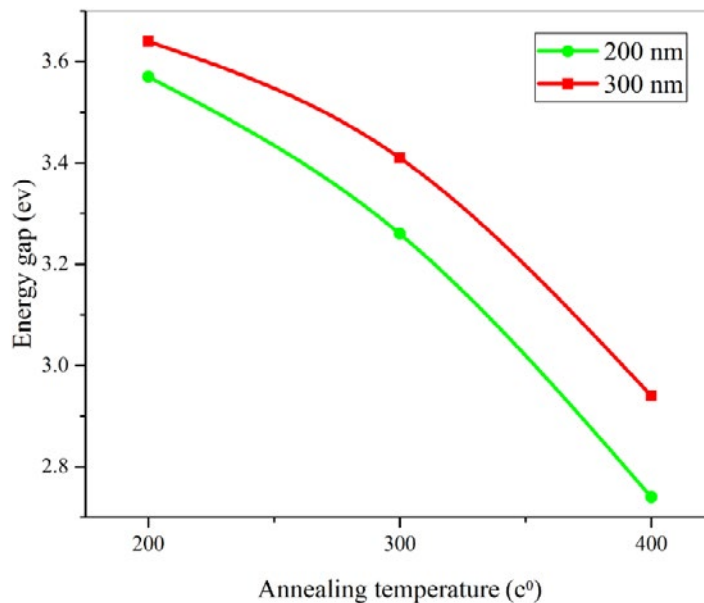


Fig. 10. Energy gap of WO<sub>3</sub> depends on annealing temperature.

mΩcm. Similar behavior of the sheet resistance of 40 keV nitrogen implanted tantalum film on glass for doses ranging from  $5 \times 10^{16}$  to  $3 \times 10^{17}$  ions/cm<sup>2</sup> has been reported elsewhere [30]. Fig. 9 shows the I-V curves obtained for unplanted and implanted samples. It can be recognized that linear I-V curves are achieved. The values of average resistance for all samples are presented in Table 4 (last column). The results show that average resistance increases with nitrogen ion dose.

This can be attributed to the transition of metal phase to nitride metal phase by nitrogen ion implantation method and increasing of nitrogen ion dose. Additionally, the energy gap of WO<sub>3</sub> samples with 200 and 300 nm in size, determined with UV- visible (Fig. 10) reveals that as annealing temperature increases, the energy gap reduced. It means energy gap of WO<sub>3</sub> at higher temperature, around 800- 900°C could be so small and cannot be as n-type semiconductor, while Ta/N can stand even high temperature

## CONCLUSION

XRD technique investigated tantalum nitride produced by nitrogen ion implantation in Tantalum with different fluxes Diversifying from  $1 \times 10^{17}$  into  $1 \times 10^{18}$  ions/cm<sup>2</sup>, applied to obtain the structural characteristics, while the AFM technique was employed to concern the morphology of the surfaces of the samples. We can see from the above commentary that there is a structural correlation between different tantalum nitrides. XRD analysis confirms the successful establishment of tantalum nitride phase which is promoted by increasing ion implantation dose. Nitrogen ion implantations of the samples with different fluxes lead to get a functionalized surface with much more trap centers and as an exemplary cathode. The shift and broadening of the peak are associated with, produced by super nitrogen saturation and related stress caused by the nitrogen remaining in solid solution in the lattice. For ion-implanted sample at  $1 \times 10^{17}$  ions/cm<sup>2</sup>, new phases are not perceived. At a higher dose of  $(3-5) \times 10^{17}$  ions/cm<sup>2</sup> many additional peaks are observed are due to FCC TaN<sub>0.43</sub>, Ta<sub>3</sub>N<sub>5</sub> and bcc tantalum phases respectively.

The results show that TaN<sub>0.43</sub> phase of Tantalum nitride formed with nitrogen ion implantation, and intensity of this peak increases with nitrogen doses. Furthermore enhancing nitrogen flux increased surface roughness and average resistance of samples. The electrical resistivity of

tantalum of implanted samples especially after increasing ion dose increased. This cathode with more trap centers and possible surface dangling bonds can be advised for the future of ECD and nanoelectronic devices.

## CONFLICT OF INTERESTS

The authors declare that there is no conflict of interests regarding the publication of this paper.

## REFERENCES

1. Litkoti HR, Bahari A, Ojani R. Synthesis of Pt-Ni-Fe/CNT/CP nanocomposite as an electrocatalytic electrode for PEM fuel cell cathode. *Journal of Nanoparticle Research*. 2017;19(8).
2. Hoseinzadeh S, Ghasemiasl R, Bahari A, Ramezani AH. The injection of Ag nanoparticles on surface of WO<sub>3</sub> thin film: enhanced electrochromic coloration efficiency and switching response. *Journal of Materials Science: Materials in Electronics*. 2017;28(19):14855-63.
3. Dastan D, Panahi SL, Chaure NB. Characterization of titania thin films grown by dip-coating technique. *Journal of Materials Science: Materials in Electronics*. 2016;27(12):12291-6.
4. Hoseinzadeh S, Ghasemiasl R, Bahari A, Ramezani AH. n-type WO<sub>3</sub> semiconductor as a cathode electrochromic material for ECD devices. *Journal of Materials Science: Materials in Electronics*. 2017;28(19):14446-52.
5. Najafi-Ashtiani H, Bahari A, Gholipour S, Hoseinzadeh S. Structural, optical and electrical properties of WO<sub>3</sub>-Ag nanocomposites for the electro-optical devices. *Applied Physics A*. 2017;124(1).
6. Hoseinzadeh S, Ghasemiasl R, Bahari A, Ramezani AH. Effect of Post-annealing on the Electrochromic Properties of Layer-by-Layer Arrangement FTO-WO<sub>3</sub>-Ag-WO<sub>3</sub>-Ag. *Journal of Electronic Materials*. 2018;47(7):3552-9.
7. Sanghera HK, Sullivan JL, Saied SO. A study of nitrogen implantation in aluminium—a comparison of experimental results and computer simulation. *Applied Surface Science*. 1999;141(1-2):57-76.
8. Zhang J, Tu J-p, Zhang D, Qiao Y-q, Xia X-h, Wang X-l, et al. Multicolor electrochromic polyaniline-WO<sub>3</sub> hybrid thin films: One-pot molecular assembling synthesis. *Journal of Materials Chemistry*. 2011;21(43):17316.
9. Ramezani AH, Hantehzadeh MR, Ghoranneviss M, Darabi E. Structural modification of tantalum crystal induced by nitrogen ion implantation. *Bulletin of Materials Science*. 2016;39(3):633-40.
10. Budzyński P, Kamiński M, Wiertel M, Pysznik K, Drożdżel A. Mechanical Properties of the Stellite 6 Cobalt Alloy Implanted with Nitrogen Ions. *Acta Physica Polonica A*. 2017;132(2):203-5.
11. Liu Y, Zu X, Qiu S, Huang X. Improvement of tribological behavior of a Ti-Al-V alloy by nitrogen ion implantation. *Rare Metals*. 2006;25(6):309-14.
12. Choi S, Kang J, Park J, Kang Y-C. Tin nitride thin films fabricated by reactive radio frequency magnetron sputtering at various nitrogen gas ratios. *Thin Solid Films*. 2014;571:84-9.
13. Firouzabadi SS, Naderi M, Dehghani K, Mahboubi F. Effect

- of nitrogen flow ratio on nano-mechanical properties of tantalum nitride thin film. *Journal of Alloys and Compounds*. 2017;719:63-70.
14. Firouzabadi SS, Dehghani K, Naderi M, Mahboubi F. Numerical investigation of sputtering power effect on nano-tribological properties of tantalum-nitride film using molecular dynamics simulation. *Applied Surface Science*. 2016;367:197-204.
  15. Litkahi HR, Bahari A, Ojani R. Pt/Fe/NiO on CNT/CP substrate as a possible electrode of nano chip devices. *Journal of Materials Science: Materials in Electronics*. 2017;28(10):7360-7.
  16. Ramezani AH, Hoseinzadeh S, Bahari A. The Effects of Nitrogen on Structure, Morphology and Electrical Resistance of Tantalum by Ion Implantation Method. *Journal of Inorganic and Organometallic Polymers and Materials*. 2018;28(3):847-53.
  17. Chen GS, Chen ST. Diffusion barrier properties of single- and multilayered quasi-amorphous tantalum nitride thin films against copper penetration. *Journal of Applied Physics*. 2000;87(12):8473-82.
  18. Belii IM, Komarov FF, Tishkov VS, Yankovskii VM. Formation of chemical compounds by ion bombardment of thin transition metal films. *Physica Status Solidi (a)*. 1978;45(1):343-52.
  19. Wang WJ, Wang TM, Wang XJ. Structural changes and tribological behaviors of nitrogen ion-implanted tantalum. *Nuclear Instruments and Methods in Physics Research Section B: Beam Interactions with Materials and Atoms*. 1996;108(3):300-4.
  20. Zhou X, Dong HK, Li HD, Liu BX. Structural correlation in tantalum nitride formation by direct nitrogen implantation. *Vacuum*. 1989;39(2-4):307-8.
  21. Lee DY, Kim IS, Song JS. Effect of Heat Treatment on Structural Characteristics and Electric Resistance in Ta<sub>Nx</sub>Thin Film Deposited by RF Sputtering. *Japanese Journal of Applied Physics*. 2002;41(Part 1, No. 7A):4659-62.
  22. Yadav AD, Dubey SK, Gupta GK, Rao TKG. Structural and electrical properties of high dose nitrogen implanted tantalum. *Radiation Effects and Defects in Solids*. 2000;153(1):25-33.
  23. Masjedi-Arani M, Salavati-Niasari M. Simple size-controlled fabrication of Zn<sub>2</sub>SnO<sub>4</sub> nanostructures and study of their behavior in dye sensitized solar cells. *International Journal of Hydrogen Energy*. 2017;42(2):858-66.
  24. Zinatloo-Ajabshir S, Mortazavi-Derazkola S, Salavati-Niasari M. Sono-synthesis and characterization of Ho<sub>2</sub>O<sub>3</sub> nanostructures via a new precipitation way for photocatalytic degradation improvement of erythrosine. *International Journal of Hydrogen Energy*. 2017;42(22):15178-88.
  25. Masjedi-Arani M, Salavati-Niasari M. Novel synthesis of Zn<sub>2</sub>GeO<sub>4</sub>/graphene nanocomposite for enhanced electrochemical hydrogen storage performance. *International Journal of Hydrogen Energy*. 2017;42(27): 17184-91.
  26. Zinatloo-Ajabshir S, Salehi Z, Salavati-Niasari M. Green synthesis of Dy<sub>2</sub>Ce<sub>2</sub>O<sub>7</sub> ceramic nanostructures using juice of Punica granatum and their efficient application as photocatalytic degradation of organic contaminants under visible light. *Ceramics International*. 2018;44(4):3873-83.
  27. Zinatloo-Ajabshir S, Mortazavi-Derazkola S, Salavati-Niasari M. Nd<sub>2</sub>O<sub>3</sub>-SiO<sub>2</sub> nanocomposites: A simple sonochemical preparation, characterization and photocatalytic activity. *Ultrasonics Sonochemistry*. 2018;42:171-82.
  28. Gholipur R, Khorshidi Z, Bahari A. Enhanced Absorption Performance of Carbon Nanostructure Based Metamaterials and Tuning Impedance Matching Behavior by an External AC Electric Field. *ACS Applied Materials & Interfaces*. 2017;9(14):12528-39.
  29. Bahari A, Berenjhan J, Sadeghi-Nik A. Modification of Portland Cement with Nano SiC. *Proceedings of the National Academy of Sciences, India Section A: Physical Sciences*. 2016;86(3):323-31.
  30. Nazon J, Sarradin J, Flaud V, Tedenac JC, Fréty N. Effects of processing parameters on the properties of tantalum nitride thin films deposited by reactive sputtering. *Journal of Alloys and Compounds*. 2008;464(1-2):526-31.
  31. Kim D-k, Lee H, Kim D, Keun Kim Y. Electrical and mechanical properties of tantalum nitride thin films deposited by reactive sputtering. *Journal of Crystal Growth*. 2005;283(3-4):404-8.
  32. Ramezani AH, Hoseinzadeh S, Sari AH. Experimental Investigation of Corrosion Improvement Implanted Ta by Ar-Ni Ions. *Journal of Nanoelectronics and Optoelectronics*. 2019;14(3):425-30.
  33. Ramezani AH, Hoseinzadeh S, Sari AH. Experimental Investigation of Corrosion Improvement Implanted Ta by Ar-Ni Ions. *Journal of Nanoelectronics and Optoelectronics*. 2019;14(3):425-30.
  34. Dastan D. Effect of preparation methods on the properties of titania nanoparticles: solvothermal versus sol-gel. *Applied Physics A*. 2017;123(11).
  35. Davoud Dastan, Nanostructured Anatase Titania Thin Films Prepared by Sol-Gel Dip Coating Technique', *J. Atomic, Molecul., Condensate Nano Phys. (JAMCNP)*. 2015;2(2):109-114..
  36. Dastan D, Banpurkar A. Solution processable sol-gel derived titania gate dielectric for organic field effect transistors. *Journal of Materials Science: Materials in Electronics*. 2016;28(4):3851-9.
  37. Dastan D, Leila Panahi S, Yengntiwar AP, Banpurkar AG. Morphological and Electrical Studies of Titania Powder and Films Grown by Aqueous Solution Method. *Advanced Science Letters*. 2016;22(4):950-3.
  38. Dastan D, Chauré N, Kartha M. Surfactants assisted solvothermal derived titania nanoparticles: synthesis and simulation. *Journal of Materials Science: Materials in Electronics*. 2017;28(11):7784-96.
  39. Hoseinzadeh S, Sahebi SAR, Ghasemiasl R, Majidian AR. Experimental analysis to improving thermosyphon (TPCT) thermal efficiency using nanoparticles/based fluids (water). *The European Physical Journal Plus*. 2017;132(5).
  40. Hoseinzadeh S, Ghasemiasl R, Havaei D, Chamkha AJ. Numerical investigation of rectangular thermal energy storage units with multiple phase change materials. *Journal of Molecular Liquids*. 2018;271:655-60.